Hydrogen production by Ammonia decomposition over Ruthenium supported on SiC catalyst

M. Pinzón, A. Romero, A. de Lucas Consuegra, A.R. de la Osa, P. Sánchez*.

Chemical Engineering Department, Faculty of Chemical Sciences and Technology, University of Castilla-La Mancha, Avda. Camilo José Cela 12, 13071 Ciudad Real, Spain.

*Corresponding author. Tel.: +34 926295300 ext: 3418; Fax:+34 926295256;

e-mail address: Paula.Sanchez@uclm.es

Abstract

A series of ruthenium catalysts using β-SiC as a support was synthesized with different metal loading (1-5 wt.% of Ru). Catalysts were characterized and tested with hydrogen production by catalytic ammonia decomposition. Additionally, the influence of calcination conditions as well as reduction temperatures (673 K and 873 K) was studied. Ru dispersion and metallic particle size were found to greatly influence catalytic activity. Moreover, calcination in a nitrogen atmosphere could remove a higher proportion of chlorine species derived from the precursor, thereby enhancing catalytic activity. Furthermore, a lower reduction temperature resulted in smaller particle sizes of ruthenium, which were more active in ammonia decomposition. Maximum intrinsic activity was obtained for a Ru size of around 5 nm. The catalyst containing 2.5 wt.% Ru, calcined in a N_2 atmosphere and reduced at 673 K resulted in excellent H_2 production from ammonia decomposition, with ammonia conversion close to 100% at 623 K was obtained. Porous SiC proved to be a suitable support for the nanosized Ru catalyst and was highly active in hydrogen production from ammonia decomposition. Moreover, this support provided good performance stability after one day of reaction.

Keywords: ammonia decomposition, hydrogen production, ruthenium catalyst, SiC support

1. Introduction

Nowadays, current energy demand is based on a system strongly dependent on fossil fuels, particularly petroleum. There are three main problems with these: they have a negative effect on the environment [1]; they are non-renewable and finite [2]; and they are characterised by centralised production in a small number of countries whose political situation is usually unstable, which affects both price and supply [3]. Consequently, a great deal of effort is being made by the scientific community to identify new energy sources and vectors to replace these fossil fuels.

In this context, hydrogen (H_2) seems to be a good candidate for meeting global energy demand. Hydrogen, known as "the eternal fuel", is used as an energy vector since there are a multitude of advantages to using it as a fuel, as it only produces water and energy as waste from its combustion [4,5]. Moreover, hydrogen is a good alternative for use as fuel cells in electricity generation, since it yields twice the amount of energy as fossil fuels [6].

However, using it as an energy carrier is limited by storage and transportation issues. As it is a gas at room temperature, storing it requires an energy compression of 7-18 kW/GJ, which entails high storage costs [7]. In addition, the US department of energy (DOE) established strict requirements for the chemical storage of hydrogen: a high storage capacity of at least 5.5 wt.% of H_2 and 40 $g \cdot L^{-1}$ of volumetric capacity [8,9].

Given these restrictions, only some compounds meet these requirements for use as carriers: methane, derivates of amines, ammonia and complex hydrides, which have been researched for storing hydrogen safely and in an economically feasible way [10,11]. Among these, there are some advantages to using NH_3 associated with i) low production costs due to its mature technology and its use in the well-known Haber-Bosch process [12] and, ii) high availability with world annual production of around 170 Mt (2019) [13].

Chemically, H_2 accounts for 17.6% of the weight of ammonia and it is a carbon-free vector [14]. Furthermore, hydrogen produced in the ammonia decomposition reaction, which is free of CO, could be directly used in PEMFC (polymer electrolyte membrane fuel cells) [10]. Complete conversion is the sole requirement when ammonia is used in fuel cell applications, but high reaction temperatures (>773 K) are necessary to achieve this. In this context, several metals such as Ru [15–22], Ir [23], Rh [24], Pd [25], Pt [25,26], Ni [14,27–29], Co [30], Fe [31,32] and Cu-Zn [33] which have been supported on different materials (Al_2O_3, CNF, CNT, SiO_2, MgO, ZrO_2, CeO_2 and La_2O_3) have been researched as potential catalysts in the ammonia decomposition reaction. Among these, ruthenium displayed the best catalytic activity with different supports [20,21,34,35]. *X. Ju et al.* [21] employed a new synthesis method to prepare highly dispersed ruthenium with small particle sizes (3.5 nm) over mesoporous MgO, with which complete conversion was obtained at 823 K. Recently, Ru supported on ceria oxide showed the greatest activity in this reaction at 723 K due to its small particle size (1.5 nm) its firm anchorage over the support and the good capacity of ceria of adsorbing ammonia [20]. These studies are indicative that the support is crucial to this reaction. Indeed, the catalytic activity of ruthenium is support-dependent [34,36–38].

Different researches have yielded interesting results obtained by using the porous form of silicon carbide (β-SiC) as a catalytic support in different catalytic reactions [39–44]. This elaborate ceramic material possesses all the physicochemical properties required for catalyst support: high thermostability, thermal conductivity and mechanical strength, as well as chemical inertness. In this paper, for the first time, Ru supported on β-SiC has been proposed as an effective catalyst for hydrogen production by ammonia decomposition. The use of porous silicon carbide in the ammonia decomposition reaction has not previously been reported in the literature although it has several properties that

makes it suitable for such a reaction, in which homogeneous temperature distribution within the catalyst is required. Therefore, the aim of this research was to study H_2 production by ammonia decomposition using a ruthenium catalyst supported on β-SiC. In light of this, reactions with Ru catalysts are structure-sensitive and the size and shape of the ruthenium particle size depend on the preparation methods. The influence of thermal treatment, metal reduction temperature and metal loading on catalytic performance were also researched.

2. Experimental

2.1 Catalysts preparation

β-SiC (25 $m^2 \cdot g^{-1}$ and 14.1 $cm^3 \cdot g^{-1}$, SICAT CATALYST), structured as pellets, was used as the catalyst support. The catalysts were prepared by the traditional vacuum impregnation method using ruthenium (III) chloride ($RuCl_3 \cdot 3H_2O$, Sigma Aldrich) as precursor.

First, 3 g of support was placed in a glass vessel and kept under vacuum at 363 K for 2 h, using a rotatory evaporator (Buchi R-210), to remove water and other impurities adsorbed on the pellets structure. Second, a solution of ruthenium chloride in 3 mL distilled water was incorporated drop by drop over the pellets, with appropriate amounts of metal precursor to obtain catalysts with Ru loadings of 1, 2.5 and 5 wt.%. Third, the solvent was removed under vacuum at 363 K until the complete evaporation of the solution. This step was repeated for three times.

Afterwards, the catalysts were dried at 353 K overnight and subsequently calcined at 773 K for 1 h (10 $K \cdot min^{-1}$) under different atmospheres: static air furnace (Nabertherm HTC 03/15), air flow (50 $mL \cdot min^{-1}$) and N_2 flow (50 $mL \cdot min^{-1}$) using a vertical reactor located inside a tubular furnace (Lenton). Finally, the samples were reduced at two different

temperatures (673 K and 873 K, 10 K·min^{-1} heating rate) with a 50 v/v.% H_2/Ar flow (100 mL·min^{-1}) for 1 h prior to the reaction. Samples were denoted as *xRu/SiC*, where *x* represented nominal Ru loading.

2.2 Support/catalysts characterization

Ruthenium content was determined by ICP-AES, with an error of ±1%, using a RL Liberty Sequential Varian ICP-AES for the multi-element analysis. Prior to analysis, solid samples were dissolved in 3 mL of hydrofluoric acid, 2 mL of hydrochloric acid and 2 mL of hydrogen peroxide followed by microwave digestion (523 K). **Table 1** shows the ruthenium content of the catalysts prepared.

Table 1. Ruthenium content of the catalysts.

Sample	**1Ru/SiC**	**2.5Ru/SiC**	**5Ru/SiC**
Ru (wt.%)	1.0%	2.5%	4.4%

X-ray Powder Diffraction (XRD) patterns were recorded on a Philips X'Pert MPD with co-filtered Cu-Kα radiation (λ=1.54056 Å). The spectra were recorded from 2θ=20-80º with a 0.02º step size using an acquisition time of 4s per step. The phases were identified by comparing them with JCPDS (Joint Committee on Powder Diffraction Standards) files. The crystal size was determined on Debye-Scherrer equation (1):

$$D=\frac{K\cdot\lambda}{\beta\cdot\cos\theta} \quad (1)$$

where D is the average particle size, assuming particles are spherical, K= 0.9, λ = 0.15406 nm, β was the full width at half the diffracted peak and θ was the Bragg angle.

Metal-support interaction was studied by Fourier Transform Infrared spectroscopy (FTIR) in transmittance mode, on a SPECTRUM TWO spectrometer (Perkin Elmer Inc.) with universal refracting and diamond accessories. The analysis was ranged between 400

and 4000 cm^{-1} with a resolution of 4 cm^{-1}. Firstly, 2 mg of the sample and 100 mg of KBr (Honeywell) were ground with an agate pestle, until the sample was well dispersed, and the mixture had the consistency of fine powder. Powered mixture was placed on the diamond crystal under pressure until the transmittance remains constant. The FTIR spectra were recorded in air.

Hydrogen temperature-programmed reduction (H_2-TPR) was used to check the reducibility of the samples. H_2-TPR experiments were conducted in a commercial Micromeritics AutoChem 2950 HP analyser unit with TCD detection. Each calcined sample (*ca*. 0.15 g) was loaded into a U-shaped tube and outgassed by heating at 20 $K \cdot min^{-1}$ in argon flow of up (50 $mL \cdot min^{-1}$) to 523 K. After cooling to room temperature, the sample was reduced with a 5 v/v.% H_2/Ar gas mixture (60 $mL \cdot min^{-1}$) at a heating rate of 10 $K \cdot min^{-1}$, to 1173 K.

Transmission electron microscopy (TEM) analyses were carried out in a JEOL JEM-4000EX unit with an accelerating voltage of 400 kV. Samples were prepared by ultrasonic dispersion in acetone with a drop of the resulting suspension evaporated onto a holey carbon-supported grid. Ruthenium particle size from the TEM images evaluated as the surface-area weighted diameter ($\overline{d_s}$) was computed according to:

$$\bar{d}_s = \frac{\sum_i n_i \cdot d_i^3}{\sum_i n_i \cdot d_i^2} \quad (2)$$

where n_i represents the number of particles with diameter d_i. More than 400 particles were measured. All catalysts had a Gaussian particle distribution. Dispersion (D) was calculated as [45]:

$$D(\%) = 1.23 \sqrt{\frac{d_{at} \cdot 3.32}{\bar{d}_s}} \cdot 100 \text{ for } 20 \leq D \leq 92 \quad (3)$$

where d_{at} was the atomic diameter of Ru (d_{at} =*2.6 Å*).

2.3 Catalytic tests

Ammonia decomposition tests for the *x*Ru/SiC catalysts were carried out in a fixed-bed quartz reactor at atmospheric pressure under a gas hourly space velocity (GHSV) of 60000 $mL \cdot g_{cat}^{-1} \cdot h^{-1}$ operating at 523-723 K. 0.1 g of catalyst sample in pellets form (3 mm length and 1 mm diameter), was packed on a fritted quartz plate located in the middle of the reactor (10 mm i.d. and 50 mm of length).

The temperature of the catalysts was measured with a K-type thermocouple (Thermocoax) placed inside the inner quartz tube. The entire reactor was placed in a tubular furnace (*Hornos Electricos A.T.)* equipped with a temperature-programmed system. Reaction gases were Air Liquide certified standards of H_2 (99.999% purity), N_2 (99.9999% purity), Ar (99.999% purity) and NH_3 (5.000% purity). The gas flows were controlled by a set of calibrated mass flow meters (Brooks 5850 E). In this reaction system, temperature was increased to the desired (for instance to 573 K) value with a ramping rate of 4.2 $K \cdot min^{-1}$. At each experimental temperature, the reaction was running until the steady state was achieved and this period usually takes 39 min. All the pipes were heated to 353 K to prevent any ammonia condensation and, in turn, corrosion.

Firstly, the catalysts were reduced with a flow consisting of a 50 v/v.% H_2/Ar gas mixture (100 $mL \cdot min^{-1}$) at 673 K or 873 K for 1 h (10 $K \cdot min^{-1}$). After cooling to 523 K under Ar flow up, a 5 v/v.% of the NH_3 (100 $mL \cdot min^{-1}$) was fed into the reactor. Catalytic activity was then studied in the 523-723 K temperature range. Reaction products were analysed on-line by using a gas chromatograph (Agilent 7820A) that is composed of two parallel columns that combines CP-Molsieve 5Å and CP-PoraBOND Q, each of which was connected to a thermal conductivity detector (TCD) using Ar as carrier gas. Ammonia conversion (x_{NH_3}) was calculated as follows:

$$x_{NH_3}(\%) = \frac{F_{NH_{3\,in}} - F_{NH_{3\,out}}}{F_{NH_{3\,in}}} \cdot 100 \qquad (4)$$

where $F_{NH_{3_{in}}}$ and $F_{NH_{3_{out}}}$ referred to the inlet and outlet NH_3 molar flows (mmol gas·min^{-1}), respectively. Note that the data provided in this paper were the average of three successive measurements, once the reaction stabilised at the desired temperature. Note that the ammonia conversion obtained with just the support or the blank reactor was, at 673 K, negligible.

In addition, the turnover frequency (TOF, min^{-1}) was calculated according to equation (5):

$$TOF\left(min^{-1}\right)=\frac{r_{H_2}\left(mmolNH_3\cdot g_{Ru}^{-1}\cdot min^{-1}\right)\cdot A_{Ru}\left(g_{Ru}\cdot mol^{-1}\right)}{D/100} \quad (5)$$

where r_{H2} was the formation rate of hydrogen, A_{Ru} was the atomic mass of Ru (101.07 $g_{Ru}\cdot mol^{-1}$), and D (%) was ruthenium dispersion.

Furthermore, the apparent activation energy of the catalysts was calculated from the Arrhenius plot at low conversion values (<20%), assuming that the ammonia decomposition reaction was first order and had a constant apparent reaction rate. The hydrogen formation rate ($mmolH_2\cdot min^{-1}\cdot g_{Ru}^{-1}$) was calculated from the H_2 content in the outgas stream.

The stability test for 2.5Ru/SiC catalyst calcined in a nitrogen flow atmosphere at 773 K and subsequently reduced at 673 K, was performed at 723 K for 25 hours. The corresponding data were collected continuously.

3. Results and discussion

3.1 Influence of thermal treatment.

In order to study the effect of thermal treatment on the ammonia decomposition reaction, the 2.5Ru/SiC catalyst was calcined at 773 K for one hour in different calcination atmospheres (static air, air flow and N_2 flow). The three treated catalysts were subsequently reduced in situ at 873 K.

The XRD patterns of the catalysts before reduction are shown in **Figure 1**. The non-calcined catalyst showed the main diffraction peaks corresponding to the support. The silicon carbide support showed there were two polytypes: hexagonal (α-SiC [1 1 1] at 2θ≈35.5˚) and face-centred-cubic (β-SiC [0 0 2] at 2θ≈41.4˚, [2 0 2] at 2θ≈59.9˚ and [1 1 3] at 2θ≈71.7˚), which is coherent with the results reported for a pure, self-bonded, beta silicon carbide support [46]. The main difference between the catalysts with and without calcination concerned the diffraction peaks for the ruthenium. Thus, the catalyst which was not calcined did not show any signs of RuO_2 and Ru^0 since the ruthenium formed $RuCl_3$ and/or ruthenium oxychloride, which is formed when exposed to air or heat-treated with it [47–49]. Peaks at 27.8º, 54.2º and 66º (2θ) associated with ruthenium oxide (JCPDS: 40-1290) were shown for catalysts calcined in different atmospheres. Although RuO_2 is mainly formed in an oxidant atmosphere [50], this also happens with a nitrogen flow (inert atmosphere), due to the presence of ruthenium oxychloride, that is produced during synthesis, over the surface. Furthermore, Ru^0 (2θ≈45º) was only present in a N_2 calcination atmosphere, indicating it affected the transformation of ruthenium species [49]. In addition, other authors related the chlorine content with changes in the Ru electrons. So, the catalysts with the lowest amount of chlorine were more metallic in character [51,52]. For this reason, the catalyst calcined in a nitrogen flow atmosphere might have removed a higher proportion of chlorine species, as may be concluded from the higher presence of metallic ruthenium prior to reduction. Moreover, *S. Ren et al.* [53] related the presence of metallic ruthenium after calcination in a nitrogen atmosphere to the auto-reduced effect caused by carbonaceous supports.

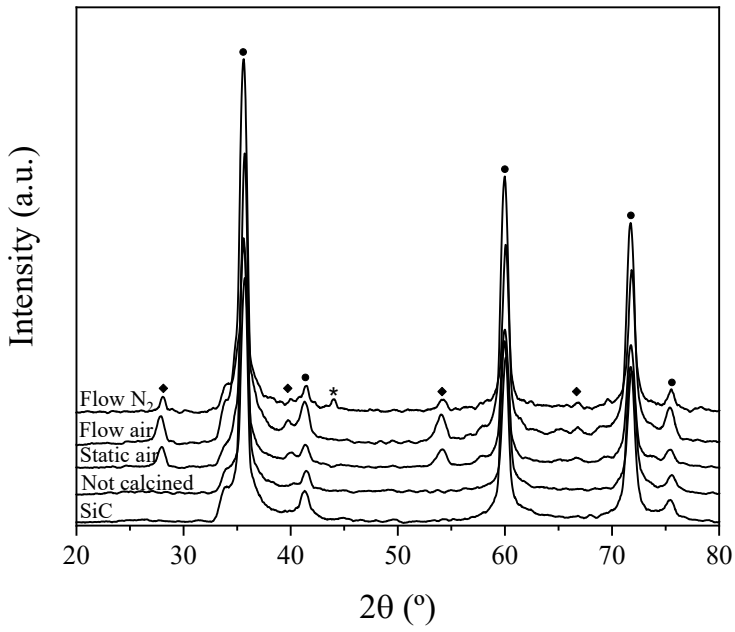

Figure 1. XRD pattern for the 2.5Ru/SiC catalyst before reduction and calcined at 773 K in different conditions: • β-SiC, ♦ RuO_2 and ∗ Ru^0.

FT-IR spectroscopy was used to explain the interaction between β-SiC and Ru. Typical FTIR absorption spectra of support and catalysts, before reduction and calcined at 773 K in different conditions, are shown in **Figure 2**. The strong peak at 825 cm^{-1} denotes symmetric stretching mode Si-C bond [44,54]. However, the possible Ru-O vibration over the support (900 cm^{-1}) was masked by the strong peak at 825 cm^{-1} [55]. Unlike for the catalyst calcined in an air atmosphere (both static and with a flow), the support, the non-calcined sample and catalyst calcined in a nitrogen atmosphere show a weak peak at 1065 cm^{-1}. This signal is associated to both asymmetric Si-O-Si and Si-O-C stretching vibrations [44,56], which are suggested to be responsible for the fixation of the metal on the β-SiC surface [57]. It may suggest that ruthenium oxychloride compounds could hinder a suitable Ru-SiC interaction. Therefore, FT-IR analysis points out that the 2.5Ru/SiC catalyst calcined in N_2 might present the highest metal-support interaction.

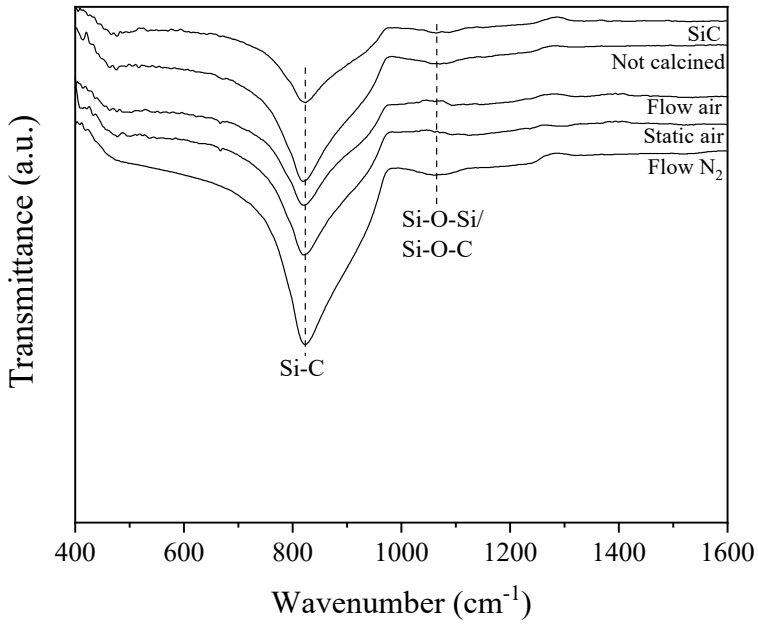

Figure 2. FT-IR spectra of 2.5Ru/SiC catalysts calcined at 773 K under different conditions.

In order to analyse the different Ru species and metal-support interaction between Ru and β-SiC, hydrogen temperature-programmed reduction experiments were carried out. H_2-TPR curves for the thermally treated catalysts are plotted in **Figure 3**. Different reduction peaks can be observed, although there are none for the SiC support, thus indicating that all H_2 consumption peaks in the catalyst profiles were related to changes in the Ru species. As can be observed, the non-calcined catalyst and that calcined in an air atmosphere (both static and with a flow) showed a peak at around 395-403 K associated with the reduction of ruthenium chloride derivates such as oxychloride [48]. However, the intensity of this signal changed with calcination. The catalyst which had not been calcinated showed the highest H_2 consumption, indicating the greatest amount of ruthenium chloride. This peak became less intense for the catalysts calcined in air (static and with flow). The catalyst calcined with an air flow showed a less intense reduction, probably due to the lower concentration of chlorine species. *Vanina accor*. [52] reported that this peak decreased when chloride content fell and affirmed that calcination at 773 K in an air atmosphere

was insufficient to remove these species. Moreover, the catalyst calcined in a nitrogen flow showed no signs of any reduction in ruthenium oxychloride and perhaps calcination in this atmosphere may be considered to be the best thermal treatment for removing chlorine species. This result is coherent with the metallic Ru character observed by the XRD in **Figure 1**. Other authors, such as *Jincan Kang et al.* [58] had similar findings for a Ru/CNT catalyst after calcination in a nitrogen atmosphere and concerning the reduction with the lowest Cl-derived/Ru ratio.

In addition, the catalysts calcined in air showed a second reduction in the peak at 440 K while the main peak of the catalyst calcined in a N_2 atmosphere was at 464 K, both of which were related to the reduction in RuO_2 species [15,59]. The displacement and greater intensity of the peak for the catalyst calcined in a nitrogen atmosphere may have been associated with higher metal-support interaction [60–62].

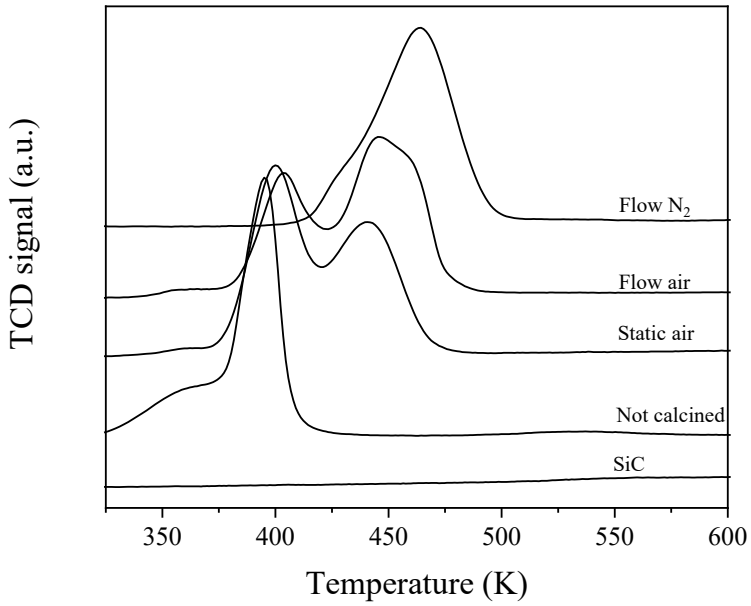

Figure 3. H_2-TPR for the 2.5Ru/SiC catalyst calcined at 773 K under different conditions.

Considering the negative effect the chloride species has on the ammonia decomposition reaction, the catalyst calcined with a nitrogen flow was expected to show better catalytic activity.

The ammonia conversion values vs. reaction temperature for the 2.5Ru/SiC catalysts obtained with different thermal treatments is shown in **Figure 4**. Ammonia conversion for all samples rose with the reaction temperature due to the endothermic nature of the decomposition, which was associated with an enthalpy of reaction of 46 $kJ \cdot mol^{-1}$ of ammonia [28,33,63]. It was seen that, in the absence of a metallic phase, any significant chemical reaction occurred after thermal ammonia decomposition, which starts at 723 K. The raw catalyst (uncalcined) and the samples calcined in an air atmosphere showed similar behaviour. However, the catalysts calcined in a nitrogen atmosphere displayed greatest NH_3 conversion, especially at lower reaction temperatures. These achieved ammonia conversion of around 97% at 723 K. The slightly lower activity of the catalysts which had not been calcined and those calcined in an air atmosphere could have been linked to the higher presence of ruthenium oxychloride, which was coherent with the temperature-programmed reduction experiments. *V. Mazzieri et al.* [48] demonstrated that chloride species were not totally removed during the calcination and reduction stages. It was suggested that these compounds inhibited the ammonia decomposition reaction, due to the reduction in electron density of the Ru sites [15,64]. Calcination in a nitrogen atmosphere removed the highest amount of chlorine, which led to greater activity in Ru. This, in turn, improved hydrogen production from ammonia, which was in agreement with the XRD and TPR characterization of this catalyst.

Therefore, the nitrogen flow calcination atmosphere was selected as the most appropriate thermal treatment for the catalysts described herein due to their use in the ammonia decomposition reaction.

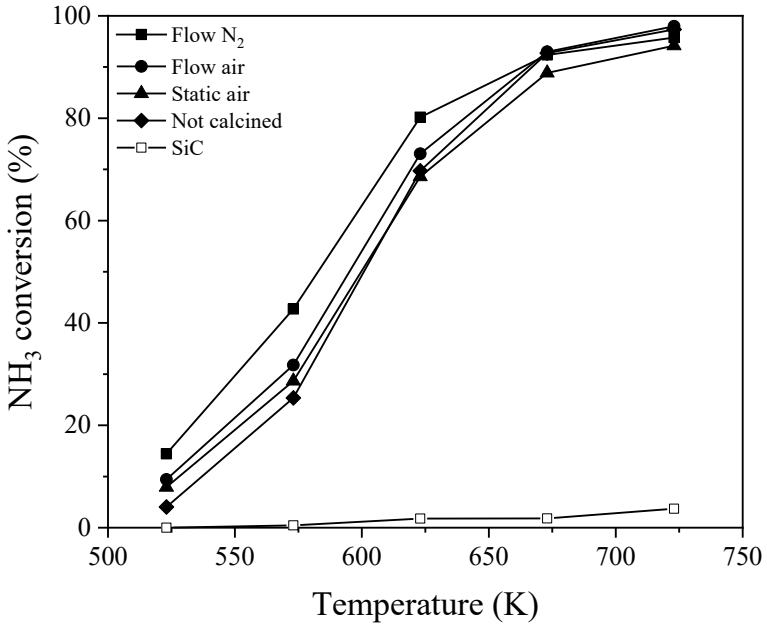

Figure 4. NH_3 conversion of the 2.5Ru/SiC catalyst calcined at 773 K in different conditions and reduced at 873 K.

3.2 Influence of reduction temperature and metal loading.

Two different reduction temperatures (673 and 873 K) and three ruthenium loadings (1, 2.5 and 5 wt.%), calcined at 773 K in a N_2 flow atmosphere, were tested for hydrogen production from ammonia with ruthenium supported with a silicon carbide catalyst.

Firstly, H_2-TPR analysis were carried out to identify the reduction effects the Ru/SiC catalysts had with different loadings of ruthenium. The H_2-TPR profiles for the synthesized samples are plotted in **Figure 5**. As can be seen, all the catalysts displayed a single H_2 consumption peak at around 394-480 K, which was related to the reduction in ruthenium species, mainly RuO_2, to metallic Ru [19,36,38]. As expected, an increase in Ru loading increased the size of the RuO_2 clusters, thereby increasing the intensity of the reduction peak, which implied a greater reduction in ruthenium oxide [65,66]. Moreover, as Ru loading increased, the peak shifted to higher temperatures as reducing the Ru species became more difficult. In light of the TPR results obtained, it may be concluded

that, at reduction temperatures higher than 550 K and after calcination in a nitrogen flow atmosphere, ruthenium is mostly reduced to Ru^0.

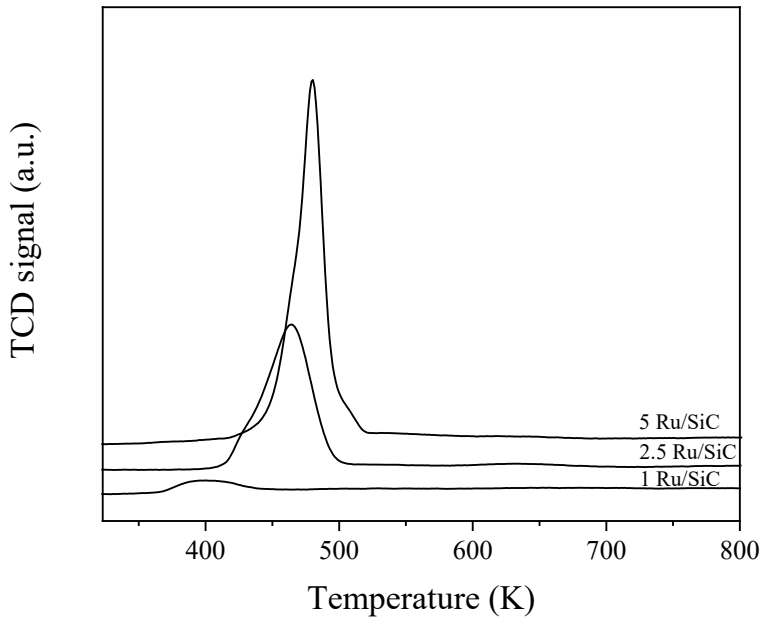

Figure 5. H_2-TPR of catalysts with different ruthenium loadings and calcined in a N_2 flow atmosphere at 773 K.

Additionally, since different authors [67–69] have found that Ru nanoparticles tend to agglomerate in thermal treatment, these catalysts, which were synthesized by varying the metal content, were reduced at two different temperatures: 673 K and 873 K.

The crystalline structure of the catalyst after reduction was studied by powder XRD (**Figure 6**). With the 1Ru/SiC catalyst, regardless of reduction temperature, the only phase observed was that of the β-SiC support. Moreover, there was no evidence of ruthenium species due to the low degree of metal loading and the high dispersion of ruthenium nanoparticles in this catalyst [20,61,65]. Furthermore, the 2.5Ru/SiC and 5Ru/SiC catalysts not only showed the diffraction peaks for the porous silicon carbide support but also peaks at 38º, 44º, 70º, 84º and 86º (2θ), which were attributed to Ru^0 (JCPDS 06-0663) [70,71]. However, these peaks were more intense when increasing both

Ru loading and reduction temperature, thereby implying higher particle size [71] was a result of the agglomeration of neighbouring Ru nanoparticles [67–69].

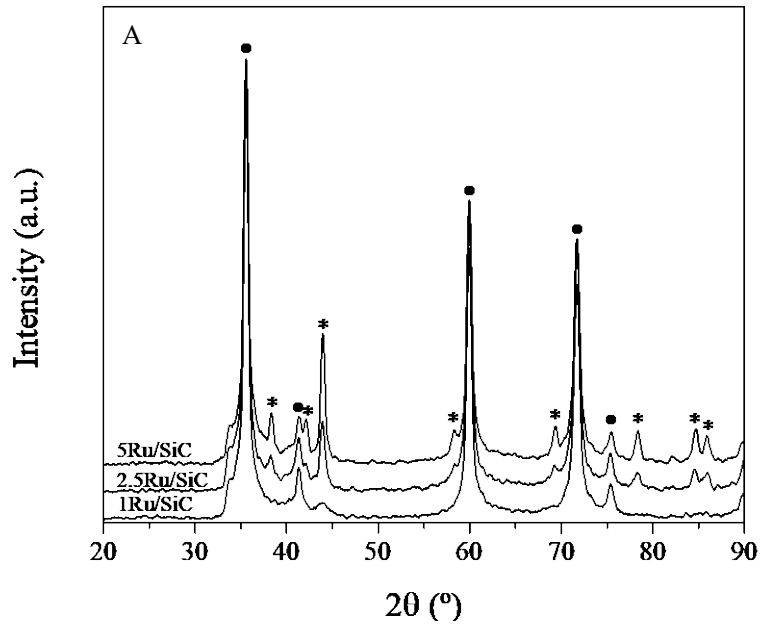

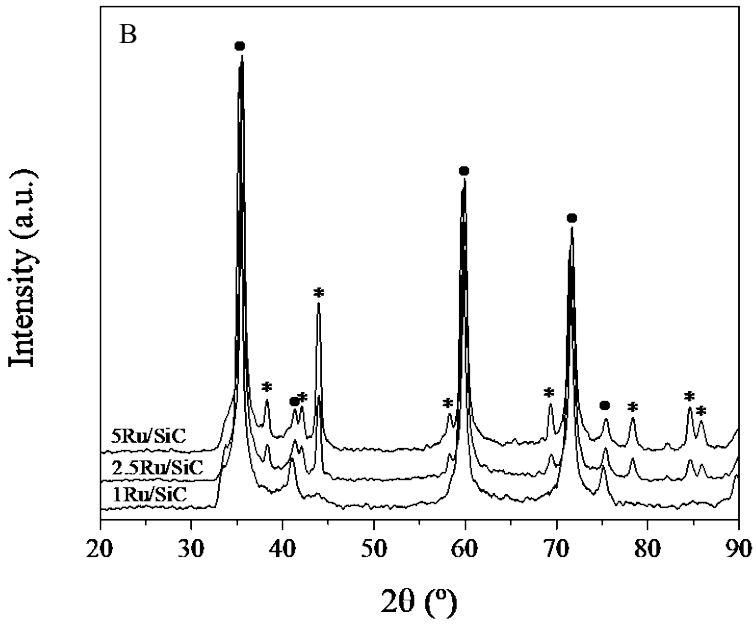

Figure 6. XRD pattern of the catalysts calcined in a N_2 atmosphere and reduced at A: 673 K and B: 873 K, where: • β-SiC and ∗ Ru^0.

Once the *x*Ru/SiC catalysts, reduced at 673 K and 873 K, were characterized by XRD, in order to obtain more information about the Ru particle size and shape, a TEM analysis was carried out.

TEM images of the catalysts after reduction at different reduction temperatures and with different ruthenium loadings are shown in **Figure 7** and **Figure 8**. In all samples, well dispersed nanosized Ru particles hemispherical or hexagonal in shape, were obtained. Ru particle size and dispersion of each sample at different reduction temperatures are summarized in **Table 2**. Note the catalyst reduced at 673 K with the lowest Ru loading (1 wt.%) showed a very small ruthenium particle size (1.75 nm) and the highest dispersion (86.4 %) value, which is in keeping with the XRD patterns for the reduced catalysts (**Figure 6).** An increase in ruthenium loading produced an increase in particle size, and, consequently, lower dispersion. With respect to reduction and according to different authors [67,68], Ru crystallites agglomerate when the reduction temperature is increased, which leads to less metal dispersion. On observation of the particle size distribution curves (**Figure 7** and **Figure 8**), it might be concluded that a narrow distribution (related to a more homogeneous particle size) was obtained when there was a low reduction temperature and metal loading below 5 wt.%. Additionally, this support (β-SiC) enabled high Ru dispersion to be obtained despite its low specific surface area (25 $m^2 \cdot g^{-1}$) [72].

Table 2. Ru particle size and dispersion of catalysts.

	Reduction temperature	$\overline{ds}$ **(nm)**	**D (%)**
1Ru/SiC	673 K	1.75	86.4
	873 K	3	65.9
2.5Ru/SiC	673 K	5	51.1
	873 K	7.5	41.7
5Ru/SiC	673 K	7	43.2
	873 K	12.5	32.3

Calcination conditions: 773 K in a N_2 atmosphere.

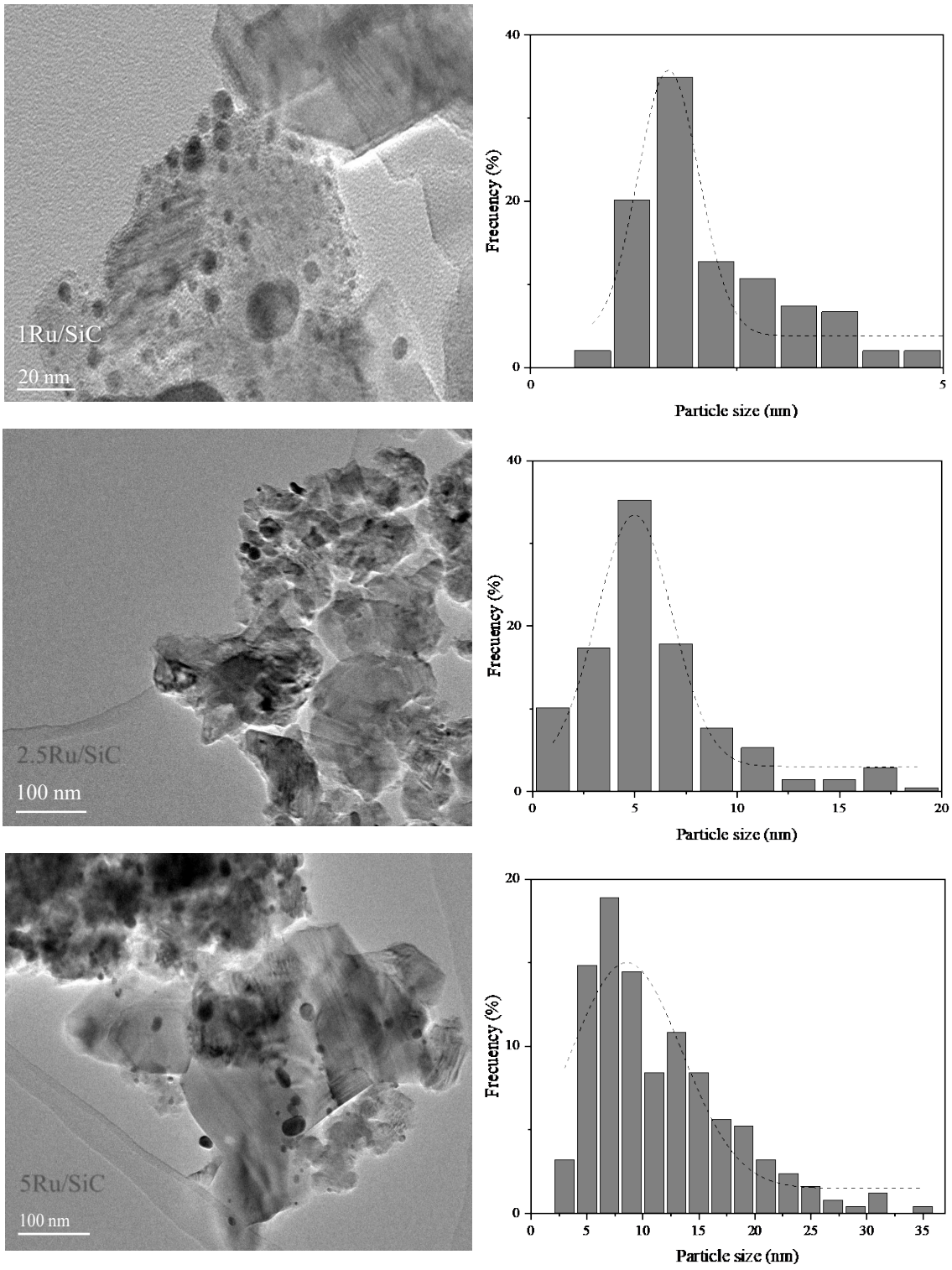

Figure 7. TEM images and particle size distributions of samples reduced at 673 K.

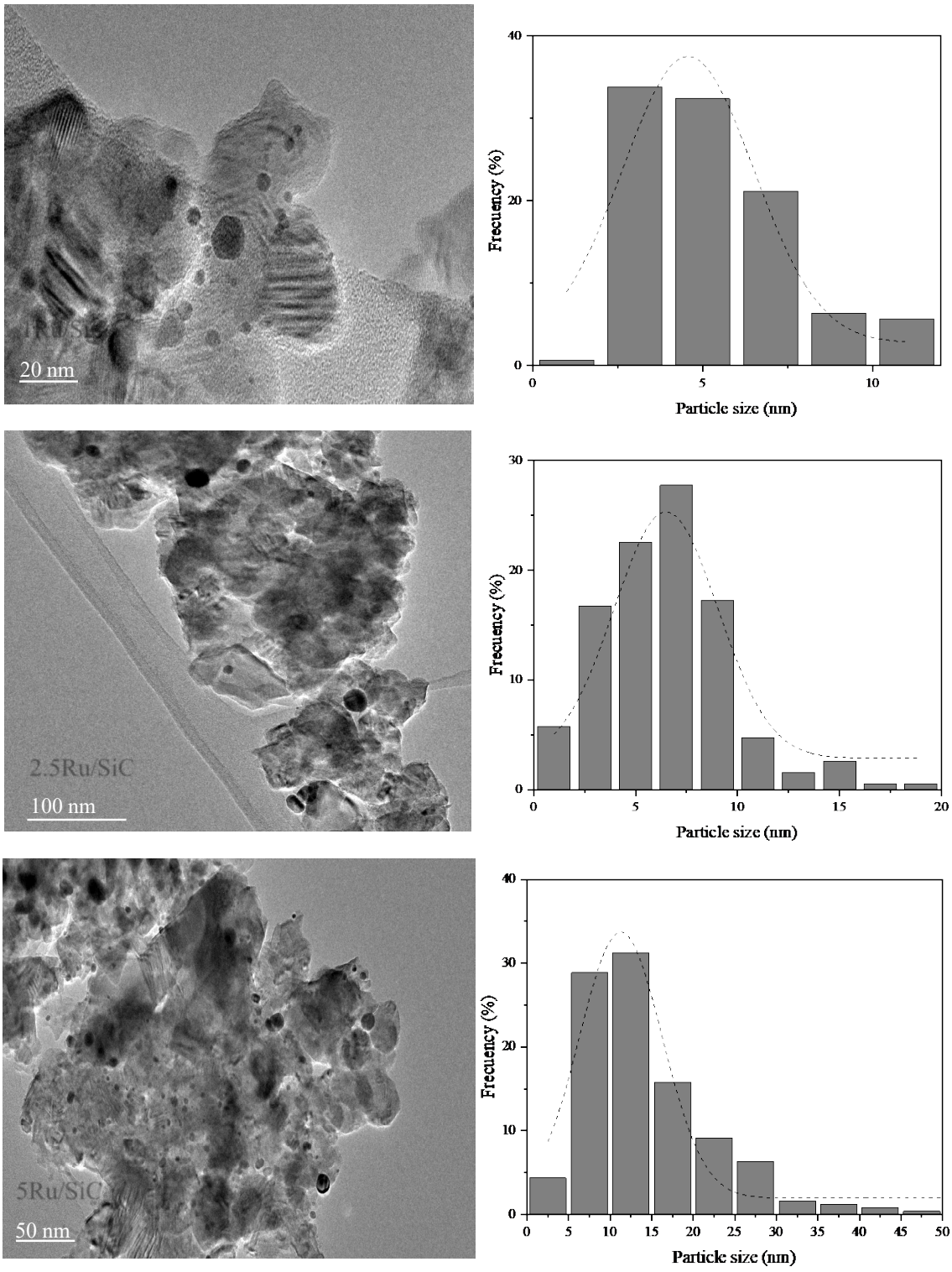

Figure 8. TEM images and particle size distributions of samples reduced at 873 K.

In order to analyse the influence of Ru loading and reduction temperature on the catalysts using β-SiC as the support, several experiments on the ammonia decomposition reaction were carried out. In **Figure 9,** ammonia decomposition conversion is plotted vs. the

reaction temperature obtained using the 1Ru/SiC, 2.5Ru/SiC and 5Ru/SiC catalysts reduced at two different temperatures. Ammonia conversion is known to increase with ruthenium loading until a certain value is reached [71,73]. In this study, when Ru loading increases up to 5 wt.%, ammonia conversion remained almost unaffected for both reduction temperatures due to blockage and possible inhibition of the active sites. These findings concurred with those reported by other authors [34,71]. In contrast, a metal loading lower than 1 wt.% seemed to be insufficient for providing enough catalytic active sites [61]. Note, the catalysts synthetized with the same Ru content (but reduced at 673 K) displayed higher activity than those reduced at 873 K. This difference in catalytic activity may have been related to the lower ruthenium particle size and higher dispersion achieved when the catalysts were reduced at a lower temperature (i.e. 673 K). In view of this, it appears the ammonia decomposition reaction with Ru catalysts is a structure-sensitive one [67,71,74–76]. Moreover, it is essential for determining an optimal loading of Ru with a given particle size and a good degree of dispersion so as to maximise catalytic activity. In this respect, some authors have suggested that a Ru particle size of between 3 and 5 nm leads to a higher concentration of B5 (which are made up for one layer consisting in three ruthenium atoms and a layer directly above it containing two more atoms [67]) type sites, and, in turn, higher ammonia conversion [30,38,67,77]. Furthermore, other authors have indicated that not only the size but also the shape of the ruthenium nanoparticles is important when obtaining these active sites. For the Ru/Al_2O_3 catalyst, Ru active B5 sites peaks at 7 nm for elongated nanoparticles whereas this occurs at 1.8-3 nm for hemispherical nanoparticles [77]. *L.Li et al.* [61] synthesized ruthenium with Cr_2O_3 as the support with a particle size of 4 nm hemispherical in shape, which reached complete ammonia conversion at 873 K. In this paper, in which β-SiC was used as the support, all the catalysts showed hemispherical or hexagonal Ru nanoparticles, as

seen in the TEM images (**Figure 7 and Figure 8**). Thus, differences in the catalytic performance of *x*Ru/SiC could be associated with the concentration of active sites in relation to particle size and not to their shape.

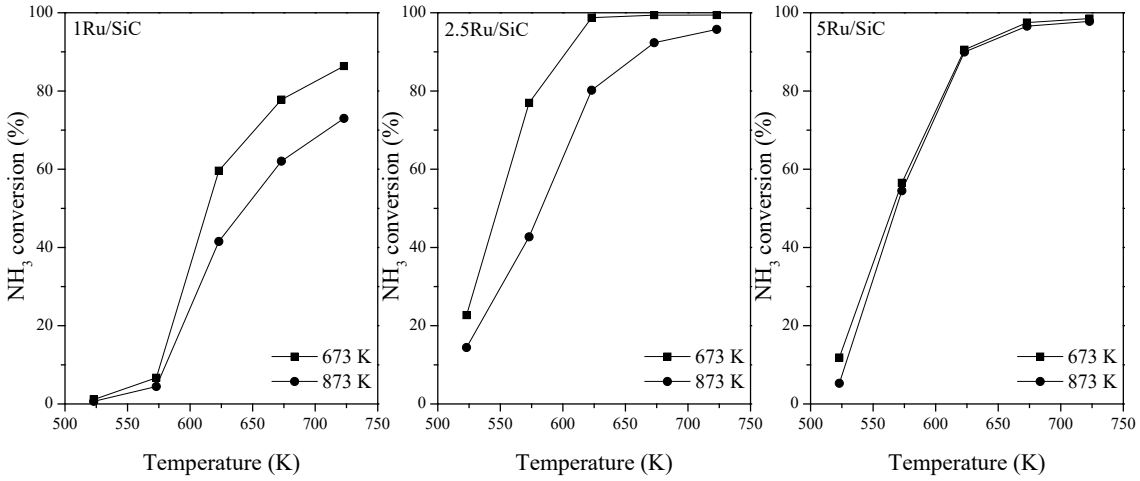

Figure 9. NH_3 conversion of the catalysts calcined at 773 K in a N_2 atmosphere and reduced at different temperatures.

In order to determine the influence of metal particle size on the intrinsic activity of the *x*Ru/SiC catalysts, the TOF values of each sample were calculated as detailed in section 2.3 and represented according to particle size (**Figure 10**). H_2 production peaked at around 5 nm for the samples reduced at 673 K, which shifted to a higher particle size at a higher reduction temperature. As expected, the samples reduced at lower temperatures showed better intrinsic activity. As mentioned above, this suggested that ammonia conversion with the Ru catalysts was very dependent on the particle size of the metal as reported by other authors [38,61,67,71,77].

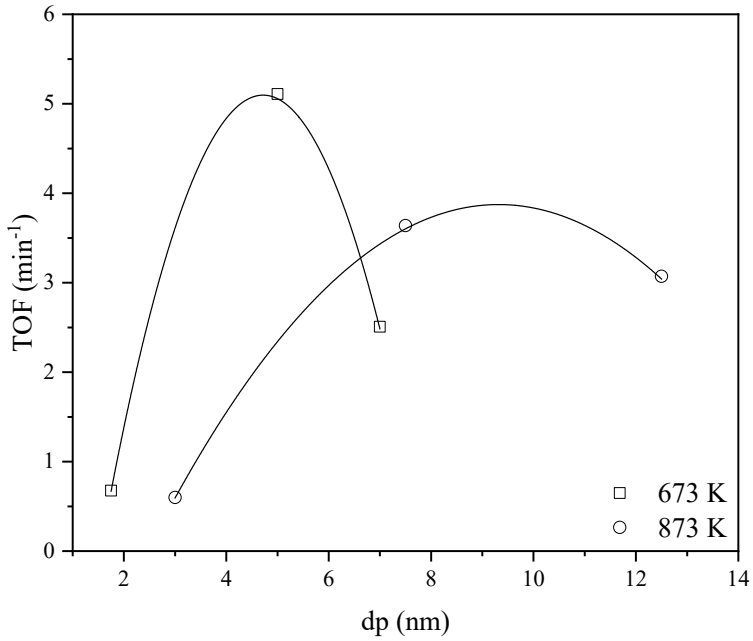

Figure 10. Intrinsic activity (TOF) *vs* Ru particle sizes in NH_3 decomposition at 573 K.

Note that with the 2.5Ru/SiC catalyst, reduced at 673 K and calcined with a N_2 flow, 99% conversion was obtained at a low reaction temperature of 623 K, which is a promising result in comparison with those from the Ru-supported catalysts in ammonia decomposition reactions, as reported in the available literature [18,37,61,78,79]. This catalyst (with an average particle size i.e. 5 nm and a dispersion of 51.1%) seems to have the optimal characteristics for producing a higher amount of B5 type sites over SiC, which are very active in the reaction.

Catalytic activity of the catalyst presented in this work was compared to that available in the literature and summarized in **Table 3**. Note that, the catalytic activity was evaluated on the basis of the gas composition feed. Nevertheless, other experimental factors (support, promoters, gas hourly space velocity, etc) obviously have an impact on the reported ammonia conversion. Different supports under the same reaction conditions show different catalytic activity, which was associated with a strong metal-support interaction and good stability [80,81].

The 2.5Ru/SiC catalyst calcined at 773 K in a N_2 atmosphere and reduced at 673 K exhibits a catalytic activity similar to that obtained with other supports under similar reaction conditions. However, the NH_3 conversion obtained with this catalyst was superior due to its optimal characteristic (above mentioned). Indeed, this catalyst with 2.5 wt.% Ru load showed 99.3% ammonia conversion and 83.4 mmol $H_2 \cdot g_{Ru}^{-1} \cdot min^{-1}$, which is more than ten times higher than the H_2 production obtained by Ru/MgO and Ru/$Ba(NH_2)_2$ catalysts, with around 5 wt.% ruthenium load, at the same gas hourly space velocity [81] and pure ammonia. On the other hand, the catalysts with 1 wt.% Ru over SBA 200-γ-Al_2O_3 showed a higher ammonia conversion due to the lowest feed ammonia composition (1 v/v.%) [82].

Table 3. Comparison of catalytic activity over Ru-based catalysts for the ammonia decomposition reaction at 673 K.

Support	wt.% Ru	dp (nm)	Gas composition	GHSV ($mL \cdot g_{cat}^{-1} \cdot h^{-1}$)	NH_3 conversion (%)	H_2 formation rate (mmol $H_2 \cdot g_{Ru}^{-1} \cdot min^{-1}$)	Ref.
SiC	2.5	5	5%NH_3-Ar	60000	99.3	83.4	This work.
SBA 200-γ-Al_2O_3	1	-	1%NH_3-Ar	30000	99.7	-	[82]
10La-Al_2O_3	0.7	3	10%NH_3-N_2	10000	20	-	[80]
MgO	4.7	2.7	5%NH_3-Ar/ Pure NH_3	60000	47/5	-/1.2	[81]
$Ba(NH_2)_2$	4.4	3.7			54/12	-/8.1	

Table 4 shows the hydrogen production rate ($mmolH_2 \cdot g_{Ru}^{-1} \cdot min^{-1}$) and the apparent activation energy (Ea) calculated from the Arrhenius plot (Ln ($mmolNH_3 \cdot g_{Ru}^{-1} \cdot min^{-1}$) *vs* 1/T) corresponding to each catalyst prepared. The higher the hydrogen formation rates, the lower the ruthenium loading. However, the 1Ru/SiC catalysts showed the lowest conversion at 623 K which is related to the higher apparent activation energy. It has

already been established that apparent Ea decreases when ruthenium loading increases [80]. This trend was also observed with the *x*Ru/SiC catalysts, which were in the range of the apparent Ea reported for the Ru catalysts [15,20,22,61,65,79,81,83] as well as for other metals such as Ni or Co [30,84-86]. However, optimum Ru loading lead to the lowest apparent Ea. As can be observed, the 2.5Ru/SiC catalyst, reduced at 673 K, presented the lowest apparent activation energy which could have been attributed to its hemispherical Ru particle size of 5 nm (the optimal Ru size for B5 sites). Moreover, with the same ruthenium content, the catalysts reduced at 673 K showed lower apparent activation energy in comparison with those reduced at 873 K, which was probably due to the higher Ru particle size (**Table 2**).

Table 4. H_2 formation rate and apparent activation energy of the catalysts.

	Reduction temperature	H_2 formation rate (mmol $H_2 \cdot g_{Ru}^{-1} \cdot min^{-1}$)[b]	Ea ($kJ \cdot mol^{-1}$)
1Ru/SiC	673 K	129.1	181.2
	873 K	91.4	197.1
2.5Ru/SiC	673 K	82.9	113.8
	873 K	70.5	126.1
5Ru/SiC	673 K	42.0	168.7
	873 K	40.5	179.0

[b]Calculated at a reaction temperature of 623 K.

Finally, in order to check how stable the optimal Ru/SiC catalyst was, it underwent a durability test carried out at 723 K over 24 hours with a 5% ammonia feed stream (**Figure 11**). Note, ammonia conversion remained almost constant at 99% and showed excellent catalytic stability at 723 K. The 2.5Ru/SiC catalyst calcined in a nitrogen flow atmosphere and reduced at 673 K proved to be stable. Also, it showed no deactivation by sintering as

a result of adequate metal-support interaction. Therefore, β-SiC is an excellent support for preparing a Ru-based catalyst for producing hydrogen from ammonia decomposition.

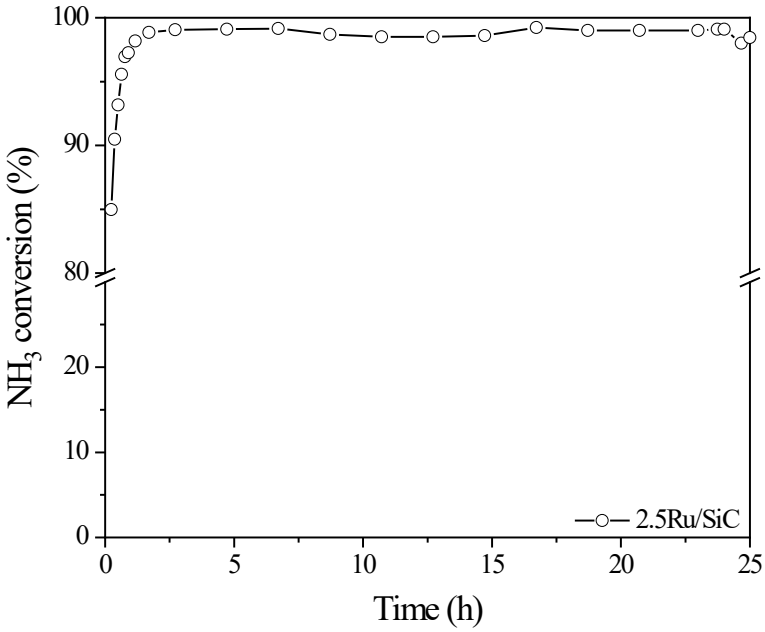

Figure 11. Stability test for the 2.5Ru/SiC catalyst calcined at 773 K in a N_2 atmosphere and reduced at 673 K (0.1 g catalyst, 60000 $mL \cdot h^{-1} \cdot g_{cat}^{-1}$ and at 723 K).

In addition, the crystalline structure of the 2.5Ru/SiC catalyst, calcined at 773 K in a N_2 atmosphere and reduced at 673 K after stability test, was studied by powder XRD (**Figure 12**). After 25 hours of reaction, the catalyst structure seems to be less crystalline, although, active phase of metallic ruthenium was presented at $2\theta=44^{o}$. Furthermore, using Scherrer equation at this peak, the average size of the Ru crystal was 15.7 and 10 nm for the catalyst before and after stability test, respectively. Thus, agglomeration did not take place suggesting that the 2.5Ru/SiC catalysts presents excellent stability for this reaction. Other authors have been observed the high stability of the ruthenium catalysts for ammonia decomposition reaction, mainly due to small Ru particle size and strong metal-support interaction [20,79,83,87].

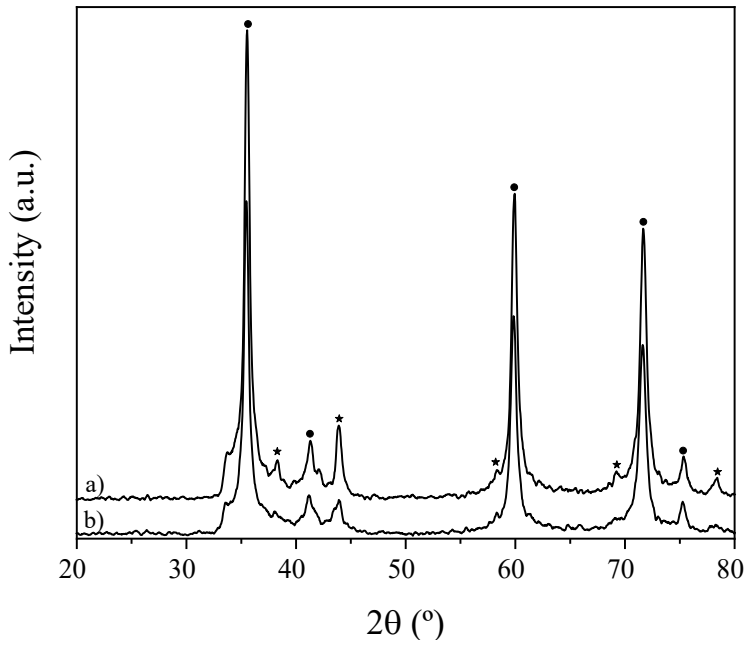

Figure 12. XRD pattern for the 2.5Ru/SiC catalyst calcined at 773 K in a N_2 atmosphere and reduced at 673 K: a) before and b) after stability test: • β-SiC and ∗ Ru^0.

4. Conclusions

It has been seen that ruthenium supported with silicon carbide is a promising catalyst in the ammonia decomposition reaction. Metal loading, calcination atmosphere and reduction temperature clearly affect the catalytic properties of *x*Ru/SiC catalysts. Thermal treatment with a N_2 flow removes a higher amount of chlorine ions, thus enhancing catalytic activity. A reduction temperature of 673 K results in low particle size and good dispersion, which, in turn, leads to better ammonia conversion. When increasing the reduction temperature, the metal particles agglomerate. The intrinsic activity of the samples peaks as Ru loading increases and an optimum size is reached (with which the particles are hemispherical or hexagonal in shape) where there are the greatest amount of active B5 sites. As a result, the catalyst with a Ru content of 2.5 wt.%, calcined with a nitrogen flow at 773 K and reduced at 673 K exhibits the best catalytic performance.

Therefore, 99% ammonia conversion is reached at a low temperature (623 K). Furthermore, this catalyst was tested over 24 hours continuously and did not display any significant reduction in performance.

5. Acknowledgements

This work was supported by the Regional Government of Castilla-La Mancha and the European Union [FEDER funds SBPLY/180501/000281].

6. References

[1] J. Imam, P.K. Singh, P. Shukla, Biohydrogen as Biofuel: Future Prospects and Avenues for Improvements, in: Biofuel Technol., Springer Berlin Heidelberg, Berlin, Heidelberg, 2013.
[2] R. Barreto, Econ. Model. 75 (2018) 196–220. https://doi.org/10.1016/j.econmod.2018.06.019.
[3] D. Parnes, Energy Econ. 78 (2019) 289–300. https://doi.org/10.1016/j.eneco.2018.11.023.
[4] R.C. Saxena, D. Seal, S. Kumar, H.B. Goyal, Renew. Sustain. Energy Rev. 12 (2008) 1909–1927. https://doi.org/10.1016/j.rser.2007.03.005.
[5] H. Seyed Ehsan, W. Mazlan Abdul, Renew. Sustain. Energy Rev. 57 (2016) 850–866. https://doi.org/10.1016/j.rser.2015.12.112.
[6] I.K. Kapdan, F. Kargi, Enzyme Microb. Technol. 38 (2006) 569–582. https://doi.org/10.1016/j.enzmictec.2005.09.015.
[7] K. Mazloomi, C. Gomes, Renew. Sustain. Energy Rev. 16 (2012) 3024-3033. https://doi.org/10.1016/j.rser.2012.02.028.
[8] J. Ren, N.M. Musyoka, H.W. Langmi, M. Mathe, S. Liao, Int. J. Hydrogen Energy 42 (2017) 289-311. https://doi.org/10.1016/j.ijhydene.2016.11.195.
[9] Targets for Onboard Hydrogen Storage for Light-Duty Vehicles, U.S. Department of Energy, Office of Energy Efficiency and Renewable Enery (2017).
[10] R. Lan, J.T.S. Irvine, S. Tao, Int. J. Hydrogen Energy 37 (2012) 1482-1494. https://doi.org/10.1016/j.ijhydene.2011.10.004.
[11] A. Klerke, C.H. Christensen, J.K. Nørskov, T. Vegge, J. Mater. Chem. 18 (2008) 2304-2310. https://doi.org/10.1039/b720020j.
[12] H. Kobayashi, A. Hayakawa, K.D.K.A. Somarathne, E.C. Okafor, Proc. Combust. Inst. 37 (2019) 109-133. https://doi.org/10.1016/j.proci.2018.09.029.
[13] L. Wood, Global Ammonia Market to 2024 - Increasing Usage for the Production of Explosives, (2019).
[14] K. Okura, K. Miyazaki, H. Muroyama, T. Matsui, K. Eguchi, RSC Adv. 8 (2018) 32102-32110. https://doi.org/10.1039/c8ra06100a.
[15] S. Armenise, F. Cazaña, A. Monzón, E. García-Bordejé, Fuel 233 (2018) 851-859. https://doi.org/10.1016/j.fuel.2018.06.129.
[16] D. Varisli, E.E. Elverisli, Int. J. Hydrogen Energy 39 (2014) 10399-10408. https://doi.org/10.1016/j.ijhydene.2014.04.207.
[17] S.F. Yin, B.Q. Xu, S.J. Wang, C.F. Ng, C.T. Au, Catal. Letters 96 (2004) 113-116. https://doi.org/10.1023/B:CATL.0000030107.64702.74.
[18] C. Huang, Y. Yu, J. Yang, Y. Yan, D. Wang, F. Hu, X. Wang, R. Zhang, G. Feng, Appl. Surf. Sci. 476 (2019) 928-936. https://doi.org/10.1016/j.apsusc.2019.01.112.
[19] Z. Wang, Y. Qu, X. Shen, Z. Cai, Int. J. Hydrogen Energy 44 (2019) 7300-7307. https://doi.org/10.1016/j.ijhydene.2019.01.235.
[20] X.C. Hu, X.P. Fu, W.W. Wang, X. Wang, K. Wu, R. Si, C. Ma, C.J. Jia, C.H. Yan, Appl. Catal. B Environ. 268 (2020) 118424. https://doi.org/10.1016/j.apcatb.2019.118424.
[21] L. Liu, G. Wu, X. Zhang, P. Yu, J. Guo, X. Ju, P. Chen, T. He, Appl. Catal. B Environ. 211 (2017) 167-175. https://doi.org/10.1016/j.apcatb.2017.04.043.
[22] S. Sayas, N. Morlanés, S.P. Katikaneni, A. Herale, B. Solami, J. Gascon, Catal. Sci. Technol. 10 (2020) 5027-5035. https://doi.org/10.1039/d0cy00686f.
[23] F.R. García-García, A. Guerrero-Ruiz, I. Rodríguez-Ramos, A. Goguet, S.O. Shekhtman, C. Hardacre, Phys. Chem. Chem. Phys. 13 (2011) 12892-12899. https://doi.org/10.1039/c1cp20287a.

[24] S.F. Yin, Q.H. Zhang, B.Q. Xu, W.X. Zhu, C.F. Ng, C.T. Au, J. Catal. 224 (2004) 384-396. https://doi.org/10.1016/j.jcat.2004.03.008.
[25] R.Y. Chein, Y.C. Chen, C.S. Chang, J.N. Chung, Int. J. Hydrogen Energy 35 (2010) 589-597. https://doi.org/10.1016/j.ijhydene.2009.10.098.
[26] W. Guo, D.G. Vlachos, Nat. Commun. 6 (2015) 1-7. https://doi.org/10.1038/ncomms9619
[27] I. Lucentini, A. Casanovas, J. Llorca, Int. J. Hydrogen Energy 44 (2019) 12693-12707. https://doi.org/10.1016/j.ijhydene.2019.01.154.
[28] L. Lawtrakul, S. Henpraserttae, S. Charojrochkul, P. Toochinda, W. Klysubun, Catal. Letters 148 (2018) 1775-1783. https://doi.org/10.1007/s10562-018-2381-9.
[29] T. Meng, Q. Xu, Y. Li, J. Chang, T. Ren, Z.-Y. Yuan, J. Ind. Eng. Chem. 32 (2015) 373-379. http://dx.doi.org/10.1016/j.jiec.2015.09.017.
[30] L. Torrente-Murciano, A.K. Hill, T.E. Bell, Catal. Today 286 (2017) 131-140. https://doi.org/10.1016/j.cattod.2016.05.041.
[31] Z.-P. Hu, L. Chen, C. Chen, Z.-Y. Yuan, Mol. Catal. 455 (2018) 14-22. https://doi.org/10.1016/j.mcat.2018.05.027.
[32] D. Varisli, C. Korkusuz, T. Dogu, Appl. Catal. B Environ. 201 (2017) 370-380. https://doi.org/10.1016/j.apcatb.2016.08.032.
[33] Š. Hajduk, V.D.B.C. Dasireddy, B. Likozar, G. Dražić, Z.C. Orel, Appl. Catal. B Environ. 211 (2017) 57-67. https://doi.org/10.1016/j.apcatb.2017.04.031.
[34] S.F. Yin, B.Q. Xu, X.P. Zhou, C.T. Au, Appl. Catal. A Gen. 277 (2004) 1-9. https://doi.org/10.1016/j.apcata.2004.09.020.
[35] S. Mukherjee, S. V. Devaguptapu, A. Sviripa, C.R.F. Lund, G. Wu, Appl. Catal. B Environ. 226 (2018) 162-181. https://doi.org/10.1016/j.apcatb.2017.12.039
[36] F.R. García-García, J. Álvarez-Rodríguez, I. Rodríguez-Ramos, A. Guerrero-Ruiz, Carbon N. Y. 48 (2010) 267-276. https://doi.org/10.1016/j.carbon.2009.09.015.
[37] A.K. Hill, L. Torrente-Murciano, Appl. Catal. B Environ. 172-173 (2015) 129-135. https://doi.org/10.1016/j.apcatb.2015.02.011.
[38] Z. Hu, J. Mahin, S. Datta, T.E. Bell, L. Torrente-Murciano, Top. Catal. 62 (2019) 1169-1177. https://doi.org/10.1007/s11244-018-1058-3.
[39] J.M. García-Vargas, J.L. Valverde, J. Díez, P. Sánchez, F. Dorado, Appl. Catal. B Environ. 164 (2015) 316-323. https://doi.org/10.1016/j.apcatb.2014.09.044.
[40] A.R. de la Osa, A. De Lucas, J. Díaz-Maroto, A. Romero, J.L. Valverde, P. Sánchez, Catal. Today 187 (2012) 173-182. https://doi.org/10.1016/j.cattod.2011.12.029.
[41] J. Díez-Ramírez, J.A. Díaz, F. Dorado, P. Sánchez, Fuel Process. Technol. 173 (2018) 173-181. https://doi.org/10.1016/j.fuproc.2018.01.024.
[42] J. Díez-Ramírez, J.A. Díaz, P. Sánchez, F. Dorado, J. CO_2 Util. 22 (2017) 71-80. https://doi.org/10.1016/j.jcou.2017.09.012.
[43] A.R. de la Osa, A. Romero, J. Díez-Ramírez, J.L. Valverde, P. Sánchez, Top. Catal. 60 (2017) 1082-1093. https://doi.org/10.1007/s11244-017-0792-2.
[44] L. Seifikar Gomi, M. Afsharpour, P. Lianos, J. Ind. Eng. Chem. 89 (2020) 448-457. https://doi.org/10.1016/j.jiec.2020.06.019.
[45] G. Peng, M. Steib, F. Gramm, C. Ludwig, F. Vogel, Catal. Sci. Technol. 4 (2014) 3329-3339 https://doi.org/10.1039/c4cy00586d.
[46] M.J. Ledoux, C. Pham-Huu, CATTECH 5 (2001) 226-246. https://doi.org/10.1023/A:1014092930183.
[47] K.V.R. Chary, C.S. Srikanth, Catal. Letters 128 (2009) 164-170. https://doi.org/10.1007/s10562-008-9720-1.
[48] V. Mazzieri, F. Coloma-Pascual, A. Arcoya, P.C. L'Argentière, N.S. Fígoli, Appl. Surf. Sci. 210 (2003) 222-230. https://doi.org/10.1016/S0169-4332(03)00146-6.
[49] L. Zhao, J. Zhou, H. Chen, M. Zhang, Z. Sui, X. Zhou, Korean J. Chem. Eng. 27 (2010) 1412-1418. https://doi.org/10.1007/s11814-010-0257-9.
[50] Koopman P.G.J., Kieboom A.P.G., Van Bekkum, H. J. Catal. 69 (1981) 172-179. https://doi.org/10.1016/0021-9517(81)90139-1.
[51] M.A. Sánchez, V.A. Mazzieri, S. Pronier, M.A. Vicerich, C. Especel, F. Epron, C.L. Pieck, J. Chem. Technol. Biotechnol. 94 (2019) 982-991. https://doi.org/10.1002/jctb.5849.
[52] V.A. Mazzieri, P.C. L'Argentière, F. Coloma-Pascual, N.S. Fígoli, Ind. Eng. Chem. Res. 42 (2003) 2269-2272. https://doi.org/10.1021/ie0209428.
[53] S. Ren, F. Huang, J. Zheng, S. Chen, H. Zhang, Int. J. Hydrogen Energy 42 (2017) 5105-5113. https://doi.org/10.1016/j.ijhydene.2016.11.010.
[54] E. Kocaman, F. Çalışkan, Mater. Chem. Phys. 256 (2020) 123716.

https://doi.org/10.1016/j.matchemphys.2020.123716.
[55] T. López, P. Bosch, M. Asomoza, R. Gómez, J. Catal. 133 (1992) 247–259. https://doi.org/10.1016/0021-9517(92)90201-R.
[56] S. Tomar, S. Gangwar, K. Kondamudi, S. Upadhyayula, Int. J. Hydrogen Energy 45 (2020) 21287–21296. https://doi.org/10.1016/j.ijhydene.2020.05.177.
[57] H. Yang, Y. Zhang, J. Zhou, Z. Wang, J. Liu, K. Cen, Int. J. Hydrogen Energy 41 (2016) 3339–3348. https://doi.org/10.1016/j.ijhydene.2015.12.042.
[58] J. Kang, W. Deng, Q. Zhang, Y. Wang, J. Energy Chem. 22 (2013) 321-328. https://doi.org/10.1016/S2095-4956(13)60039-X.
[59] H.S. Whang, M.S. Choi, J. Lim, C. Kim, I. Heo, T.S. Chang, H. Lee, Catal. Today 293-294 (2017) 122-128. https://doi.org/10.1016/j.cattod.2016.12.034.
[60] V. Pavankumar, C.S. Srikanth, A.N. Rao, K.V.R. Chary, J. Nanosci. Nanotechnol. 14 (2014) 3137-3146. https://doi.org/10.1166/jnn.2014.8544.
[61] L. Li, Y. Wang, Z.P. Xu, Z. Zhu, Appl. Catal. A Gen. 467 (2013) 246-252. https://doi.org/10.1016/j.apcata.2013.07.003.
[62] X.L. Yang, W.Q. Zhang, C.G. Xia, X.M. Xiong, X.Y. Mu, B. Hu, Catal. Commun. 11 (2010) 867-870. https://doi.org/10.1016/j.catcom.2010.03.008.
[63] J. Guo, P. Chen, Chem 3 (2017) 709-712. https://doi.org/10.1016/j.chempr.2017.10.004.
[64] S.F. Yin, B.Q. Xu, S.J. Wang, C.T. Au, Appl. Catal. A Gen. 301 (2006) 202-210. https://doi.org/10.1016/j.apcata.2005.12.005.
[65] V. Pendyala, G. Jacobs, U. Graham, J.-S. Poirier, D. Smiley, M. Morales, W. Shafer, S. Khalid, B. Davis Fischer-Tropsch Synthesis: Activity and Product Selectivity of SiC-Supported Ru Catalysts, in: Fischer-Tropsch Synth. Catal. Catal. 2016. https://doi.org/10.1201/b19455-17.
[66] P. Betancourt, A. Rives, R. Hubaut, C. Scott, J. Goldwasser, Appl. Catal. A Gen. 170 (1998) 307-314. https://doi.org/10.1016/S0926-860X(98)00061-1.
[67] F.R. García-García, A. Guerrero-Ruiz, I. Rodríguez-Ramos, Top. Catal. 52 (2009) 758-764. https://doi.org/10.1007/s11244-009-9203-7.
[68] L. Gonzalo-Chacón, M. Almohalla, E. Gallegos-Suarez, A. Guerrero-Ruiz, I. Rodríguez-Ramos, Appl. Catal. A Gen. 480 (2014) 86-92. https://doi.org/10.1016/j.apcata.2014.04.046.
[69] B. Lin, K. Wei, J. Lin, J. Ni, Catal. Commun. 39 (2013) 14-19. https://doi.org/10.1016/j.catcom.2013.05.003.
[70] W. Fu, W. Chen, G. Qian, D. Chen, W. Yuan, X. Zhou, X. Duan, React. Chem. Eng. 4 (2019) 316-322. https://doi.org/10.1039/c8re00223a.
[71] W. Zheng, J. Zhang, H. Xu, W. Li, Catal. Letters 119 (2007) 311-318. https://doi.org/10.1007/s10562-007-9237-z.
[72] Y. Huang, Y. Duan, S. Qiu, M. Wang, C. Ju, H. Cao, Y. Fang, T. Tan, Sustain. Energy Fuels 2 (2018) 637-647. https://doi.org/10.1039/c7se00535k.
[73] A.K. Hill, L. Torrente-Murciano, Int. J. Hydrogen Energy 39 (2014) 7646-7654. https://doi.org/10.1016/j.ijhydene.2014.03.043.
[74] G. Li, M. Kanezashi, T. Tsuru, Catalysts 7 (2017) 1-12. https://doi.org/10.3390/catal7010023.
[75] X.K. Li, W.J. Ji, J. Zhao, S.J. Wang, C.T. Au, J. Catal. 236 (2005) 181-189. https://doi.org/10.1016/j.jcat.2005.09.030.
[76] G. Li, H. Nagasawa, M. Kanezashi, T. Yoshioka, T. Tsuru, J. Mater. Chem. A 2 (2014) 9185-9192. https://doi.org/10.1039/c4ta01193g.
[77] A.M. Karim, V. Prasad, G. Mpourmpakis, W.W. Lonergan, A.I. Frenkel, J.G. Chen, D.G. Vlachos, J. Am. Chem. Soc. 131 (2009) 12230-12239. https://doi.org/10.1021/ja902587k.
[78] Z. Wang, Y. Qu, X. Shen, Z. Cai, Int. J. Hydrogen Energy 44 (2019) 7300-7307. https://doi.org/10.1016/j.ijhydene.2019.01.235.
[79] Z. Hu, J. Mahin, L. Torrente-Murciano, Int. J. Hydrogen Energy 44 (2019) 30108-30118. https://doi.org/10.1016/j.ijhydene.2019.09.174.
[80] D.B. Chung, H.Y. Kim, M. Jeon, D.H. Lee H.S. Park, S.H. Choi, S.W. Nam, S.C. Jang, J. Park, K. Lee, C.W. Yoon, Int. J. Hydrogen Energy 42 (2017) 1639–1647. https://doi.org/10.1016/j.ijhydene.2016.08.020.
[81] P. Yu, J. Guo, L. Liu, P. Wang, F. Chang, H. Wang, X. Ju, P. Chen, J. Phys. Chem. C. 120 (2016) 2822–2828. https://doi.org/10.1021/acs.jpcc.5b11768.
[82] K. McCullough, P.H. Chiang, J.D. Jimenez, J.A. Lauterbach, Materials (Basel.) 13 (2020) 1-20. https://doi.org/10.3390/MA13081869.
[83] Z.Whang, Z.Cai, Z.Wei, ACS Sustain. Chem. Eng 7 (2019) 8226-8235. https://doi.org/10.1021/acssuschemeng.8b06308.
[84] Z.S. Zhang, X.P. Fu, W.W. Wang, Z. Jin, Q.S. Song, C.J. Jia, Sci. China Chem 61 (2018) 1389-

1398. https://doi.org/10.1007/s11426-0.18-9261.5.
[85] T.E. Bell, H. Ménard, J.M. González Carballo, R. Tooze, L. Torrente-Murciano, Int. J. Hydrogen Energy 45 (2020) 27210-27220. https://doi.org/10.1016/j.ijhydene.2020.07.090.
[86] X.C. Hu, W.W. Wang, Z. Jin, X. Wang, R. Si, C.J. Jia, J. Energy Chem 38 (2019) 41-49. https://doi.org/10.1016/j.echem.2018.12.024.
[87] X. Ju, L. Liu, X. Zhang, J. Feng, T. He, P. Chen, ChemCatChem 11 (2019) 4161-4170. https://doi.org/10.1002/cctc.201900306.